

Nanocrystalline diamond photonics platform with high quality factor photonic crystal cavities

X. Checoury, D. Néel, P. Boucaud, C. Gesset, H. Girard et al.

Citation: *Appl. Phys. Lett.* **101**, 171115 (2012); doi: 10.1063/1.4764548

View online: <http://dx.doi.org/10.1063/1.4764548>

View Table of Contents: <http://apl.aip.org/resource/1/APPLAB/v101/i17>

Published by the [American Institute of Physics](http://www.aip.org).

Related Articles

Quasiresonant excitation of InP/InGaP quantum dots using second harmonic generated in a photonic crystal cavity

Appl. Phys. Lett. **101**, 161116 (2012)

Enhancement of photocurrent in ultrathin active-layer photodetecting devices with photonic crystals

Appl. Phys. Lett. **101**, 161103 (2012)

Lithium niobate photonic crystal wire cavity: Realization of a compact electro-optically tunable filter

Appl. Phys. Lett. **101**, 151117 (2012)

Metamaterial features in a dielectric fiber with an inserted thin cylindrical shell

Appl. Phys. Lett. **101**, 143508 (2012)

Surface label-free sensing by means of a fluorescent multilayered photonic structure

Appl. Phys. Lett. **101**, 131105 (2012)

Additional information on *Appl. Phys. Lett.*

Journal Homepage: <http://apl.aip.org/>

Journal Information: http://apl.aip.org/about/about_the_journal

Top downloads: http://apl.aip.org/features/most_downloaded

Information for Authors: <http://apl.aip.org/authors>

ADVERTISEMENT

Universal charged-particle detector
for interdisciplinary applications:

- > Non-scanning Mass Spectrometry
- > Non-scanning Ion Mobility Spectrometry
- > Non-scanning Electron Spectroscopy
- > Direct microchannel plate readout
- > Thermal ion motion and mobility studies
- > Bio-molecular ion soft-landing profiling
- > Real-time beam current/shape tuning
- > Diagnostics tool for instrument design
- > Compact linear array for beam lines

Contact OI Analytical: +1-205-733-6900



Nanocrystalline diamond photonics platform with high quality factor photonic crystal cavities

X. Checoury,^{1(a)} D. Néel,¹ P. Boucaud,¹ C. Gesset,² H. Girard,² S. Saada,² and P. Bergonzo²

¹IEF, CNRS Univ Paris Sud 11, Bâtiment 220, F-91405 Orsay Cedex, France

²CEA, LIST, Diamond Sensors Laboratory, F-91191 Gif-sur-Yvette, France

(Received 12 September 2012; accepted 15 October 2012; published online 25 October 2012)

We demonstrate a diamond photonics platform with integrated suspended waveguide-cavity structures and two dimensional photonic crystal (PhC) cavities. PhC cavities with quality factors exceeding 2800 have been fabricated using a top-down approach from thin nanocrystalline diamond films. The developed technological process allows one to access these cavities in a fully planar geometry, including light injection and collection from the outside using lensed-fibers. This diamond platform opens the road to large scale fabrication of photonics devices including optical sensor chips. © 2012 American Institute of Physics. [<http://dx.doi.org/10.1063/1.4764548>]

Diamond is an attractive material for optics and integrated photonics.¹ Its wide bandgap offers transparency in a large spectral range from ultraviolet to far infrared, together with a high refractive index. Diamond possesses a wide variety of optically active color centers that can be used as efficient internal sources.² Moreover, diamond surfaces can be functionalized for fabricating highly stable and selective biological interfaces, a property that is particularly desirable for the realization of optical biosensors.³ Finally, its high thermal conductivity and the absence of two-photon absorption phenomena in a large spectral range make diamond a material adapted to applications involving high power densities such as third harmonic generation⁴ or stimulated Raman scattering.⁵ In order for diamond to reach its full potential in photonics devices, for example, as an optical biosensor, it is necessary to confine light in high quality factor and small mode volume cavities as well as to couple light efficiently into them. A monolithic diamond photonics architecture is expected to offer more flexibility and scalability than hybrid approaches.^{6,7} Here we demonstrate a diamond photonics platform with integrated suspended waveguide-cavity structures that can be accessed in a fully planar geometry from the outside using lensed-fibers or microscope objectives. These structures are fabricated in nanocrystalline diamond films grown on a two-inch silicon wafer. These films allow large scale processing contrary to single crystalline diamond wafers whose size is smaller than one square centimeter. In this work, two dimensional photonic crystal (PhC) cavities with quality factor exceeding 2800 and modal volume near $2.1(\lambda/n)^3$ in a nanocrystalline diamond membrane have been fabricated using a top-down approach with standard semiconductor processing techniques.

Nanocrystalline diamond films were deposited using chemical vapor deposition assisted by microwave plasma (MPCVD) technique onto two-inch silicon substrates.⁸ The nanoseeding technique is used to initiate the diamond growth.⁹ The typical film thickness used in this study is 400 nm. The diamond grain size is around 10 nm near the Si

substrate and around 100 nm near the surface. The surface roughness of the 400-nm thick diamond film is around 10 nm with a peak to valley roughness that can reach 80 nm.¹⁰ This roughness prevents the use of electronic lithography technique and the achievement of high quality (Q) factor cavities due to the strong scattering at the surface. To smooth the rough polycrystalline diamond layer, a 200-nm thick hydrogen silsesquioxane (HSQ) layer is first spun coated on the rough polycrystalline diamond layer and baked on a hot plate. This results in a smooth surface silica-like layer on top of the sample. The layers are then etched using an inductively coupled plasma (ICP) reactive ion etching with oxygen and argon gases. Oxygen is used to etch the diamond, and the argon concentration is adjusted so that the etching speeds of both silica and diamond are equal (Fig. 1(a)). Once the diamond has been smoothed, silica residues are removed in hydrofluoric acid. This process is similar but simpler than the one described in Ref. 10 since it avoids the use of a mechanical polishing step. Figure 1(b) shows the measurement of the resulting surface roughness using an atomic force microscope. The root mean square (RMS) roughness is equal to 1.6 nm only, and the peak to valley roughness is below 10 nm. These values are slightly better than those reported in Ref. 10 and are not easily reached with direct mechanical polishing.¹¹

The next processing step consists in the realization of the PhC cavities and other photonic structures necessary for the coupling of light. To improve the coupling of light into

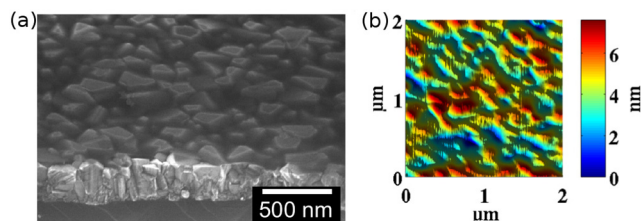


FIG. 1. (a) SEM view of a rough polycrystalline diamond layer covered by a flat silica layer during the smoothing process. (b) Atomic force microscope (AFM) image of the fully smoothed polycrystalline diamond. The measured RMS roughness is 1.6 nm.

^{a)}Electronic mail: xavier.checoury@ief.u-psud.fr.

the photonic crystals, ridge waveguides ended by inverted tapers are added at the end of the PhC as can be seen on the schematic view of the whole experimental structure in Fig. 2(a). The 200-nm wide taper tip allows to delocalize the mode field profile from the waveguide core and to increase the mode overlap with the mode of the optical fibers.¹²

Because the PhC membranes are suspended in air, we also suspended the ridge access waveguides by nanotethers. The whole structure is 500- μm long, and this architecture appears as an efficient, simple, and reproducible way to probe PhC cavity transmission in an entirely planar geometry as we already showed on silicon.^{13–15} This geometry, which requires only one lithography step and has not been yet used for coupling diamond photonic crystals from the outside, is much more compact than the ones that rely on in- and out-coupling towards the vertical direction as in Refs. 16 and 17. Because we used only standard and scalable semiconductor processing techniques, several hundreds of cavities are fabricated simultaneously, and three of them are displayed in Fig. 2(b). The equivalent angle of the air holes sidewall with the vertical direction remains below 3° as can be seen on Fig. 2(c). In silicon PhCs, such an angle theoretically allows for quality factors up to 3×10^6 .¹⁸ Figures 2(d) and 2(e) show scanning electronic microscope (SEM) views of the PhC and of a nanotether before the partial etching of the silicon substrate to free the diamond membrane. The whole fabrication process consists in the following standard steps: a 110-nm thick layer of silica is first deposited by plasma enhanced chemical vapor deposition (PECVD) on the top of the smoothed diamond layer. Electron-beam resist is then spun on the surface, and the photonic crystal and the access waveguides are patterned in the resist using electronic lithography. The pattern is transferred from the resist to silica using reactive ion etching (RIE) and then from the silica to the dia-

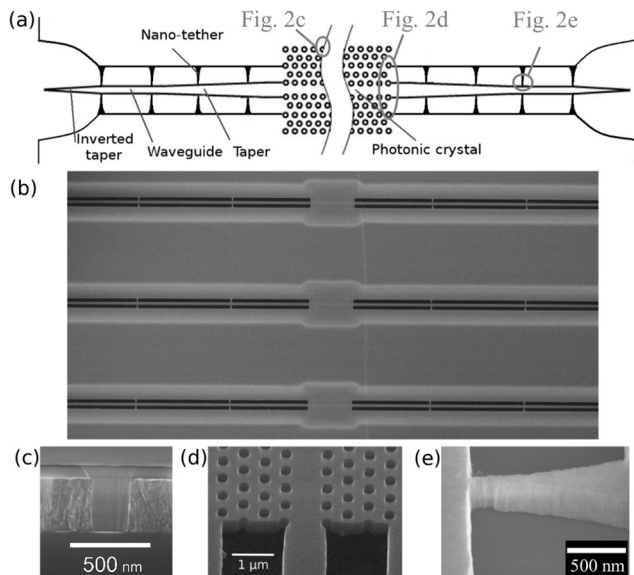


FIG. 2. Fabricated structures. (a) Schematic view of the fabricated structure. (b) SEM view of three photonic crystal cavities with their access waveguides suspended by nanotethers. (c) Cross section of an etched hole in nanocrystalline diamond layer before the removal of the silica mask. (d) Tilted view (45°) of a PhC and its access waveguide. (e) Tilted closed view of the access waveguide and a nanotether, the width of which is 70 nm at the side supporting the waveguide.

mond using an ICP RIE based on a pure O_2 chemistry. The remaining silica mask is removed in hydrofluoric acid. Finally, the silicon substrate is then partially etched to free the diamond membrane using a vapor phase isotropic XeF_2 etching process. The XeF_2 reacts with the uncovered silicon beneath the holes of the diamond structure, and the etching time is adjusted to remove 4 microns of silicon.

Electromagnetic simulations were performed to determine the geometry of the PhC cavity that can achieve high quality factors in diamond. Photonic crystal cavities as fabricated from hetero-structures¹⁹ or with a local width modulation of a line defect²⁰ are known to provide the highest quality factor Q in silicon PhC cavities with Q factor higher than 1×10^6 and modal volume of the order of $(\lambda/n)^3$. To achieve such a high quality factor, the latter cavities require the precise displacement of holes in a PhC in the nanometer range. This precision is within reach for our electronic lithography system since we recently succeeded to experimentally measure PhC cavities with quality factors up to 2×10^6 in silicon.¹³ Figure 3(a) shows the studied cavity structure in diamond made using the width modulation technique.²⁰ In fact, the cavity design is very similar to the one we realized in silicon-on-insulator.²¹ The waveguide is defined by a width equal to $0.98a\sqrt{3}$, where a is the PhC period. The four holes (red) in the center are shifted by a distance s in a direction perpendicular to the waveguide axis, and the adjacent holes (orange and yellow) are shifted by a distance of $2s/3$ and $s/3$, respectively. The photonic crystal waveguide acts as a barrier for the cavity mode, and the length of this barrier

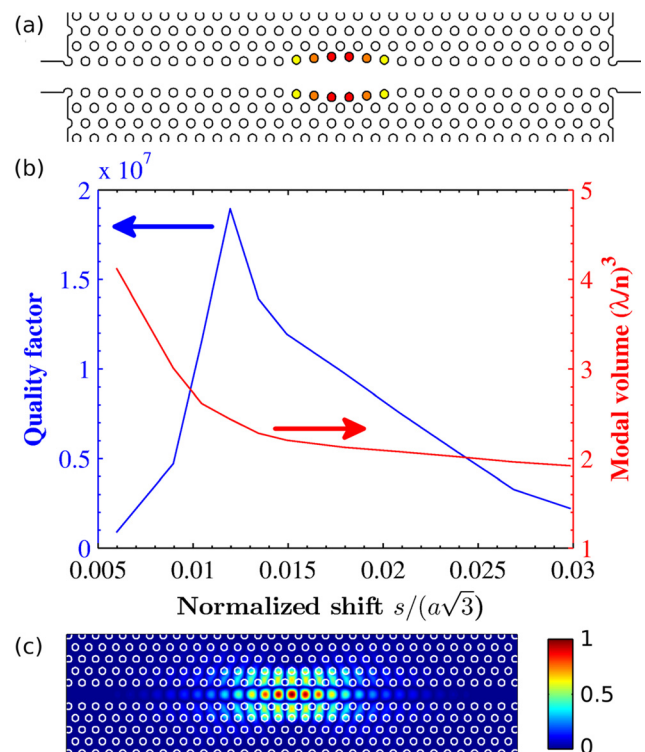


FIG. 3. Structure and simulations. (a) Structure of the cavity: the holes in warm colors define the cavity. For clarity, the shifts have been exaggerated. The red, orange, and yellow holes are shifted by a distance s , $2s/3$, and $s/3$, respectively. (b) Simulated quality factor and modal volume of the cavities as a function of the normalized shift. (c) Module of the electric field component perpendicular to the waveguide axis (arbitrary unit).

determines the coupling of the cavity to the ridge access waveguides as well as the loaded quality factor of the cavity.

We performed three dimensional finite difference in time domain (3D FDTD) simulations for PhC cavities fabricated in suspended diamond membrane and studied the Q factor evolution with the normalized shift $s/(a\sqrt{3})$ of the four central holes. The normalized hole radius r/a is equal to 0.25, the normalized membrane height h/a is equal to 0.59, and the refractive index of the diamond is assumed equal to 2.4. As seen on Fig. 3, for a normalized shift of 0.015, corresponding to a shift of 15 nm for a targeted resonance wavelength of 1550 nm, the simulated Q factor can exceed 10×10^6 , a value above the best value ever experimentally probed on a silicon photonic crystal.²² The modal volume is equal to $2.4(\lambda/n)^3$. The lower refractive index of the diamond as compared to the one of silicon does not significantly alter the Q factor but the modal volume is 40% larger in diamond than in silicon, because the resonant mode spreads more in diamond PhC barriers (Fig. 3(c)). We have checked that an increase of the membrane thickness by 10 nm results in a resonance frequency shift larger than 0.45 nm confirming that unsmoothed polycrystalline diamond membranes, with a rms roughness of 10 nm are not suitable for the achievement of high quality factor. Moreover, the quality factor remains above 1×10^6 even for a normalized displacement as high as 0.03, i.e., 30 nm for cavities with resonances at wavelengths near 1550 nm. We also checked that the Q factor remains higher than 1×10^6 if the hole radius is increased or decreased by 5% on this range of hole shifts. This contrasts with the previously reported simulation of L7-type cavities in diamond where simulated Q factors remained below 100 000^{23,24} and with micro-ring resonators that exhibit a similar Q factor but also a modal volume more than ten times greater.^{17,25} Indeed, this high Q factor is also similar to the simulated Q factor of cavities made by locally modifying the refractive index of diamond²⁶ as well as the one of nanobeam-type cavity.²⁷ However, in this last case, there is no two-dimensional (2D) photonic bandgap which is known to inhibit the spontaneous emission, a crucial property to finely control emitters.²⁸ As a consequence, these simulations show that 2D-photonic crystal cavities with Q factors of a few millions are within reach with this kind of design in diamond only if the same fabrication accuracy and material quality could be achieved on diamond as it is commonly obtained on silicon.

Before measuring the photonic crystals that have been fabricated according to the previous simulation results, suspended ridge waveguides alone have been first characterized. Two polarization maintaining lensed optical fibers with spot diameter of $\approx 2.75 \mu\text{m}$ are aligned in front of the tapers and are used to collect and inject light into the access waveguides. A tunable laser source with a 1-pm resolution is continuously tuned from 1500 nm to 1630 nm, and the transmitted power is recorded with a photodiode. Care is taken to avoid temperature variation of the sample, and the injected power in the PhC waveguide is $30 \mu\text{W}$. The inset in Fig. 4 shows the optical transmission of a single 500- μm long suspended ridge waveguide with inverted tapers at its extremities. As can be seen, the fiber-to-fiber insertion losses are 24 dB and remain constant within a ± 1 dB range over a

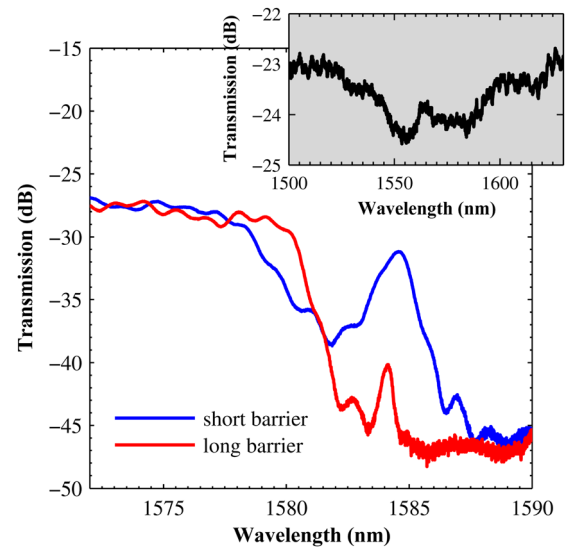


FIG. 4. Transmission spectra of the photonic crystal cavities for two barrier lengths. Inset: transmission spectrum of a single suspended ridge waveguide with its tapers.

wavelength range of 130 nm. From the measurement of similar waveguides with different lengths we deduce an insertion loss below 6 dB per taper, a value similar to the one achieved on silicon.¹³ The propagation loss is between 50 and 70 cm^{-1} , a value much higher than the one we observed in silicon for a similar geometry. As a consequence, we can expect that this propagation loss mainly results from the waveguide roughness, the material absorption, and scattering. The tethers that are 70 nm wide at the side supporting the waveguide also induce some scattering losses. If we consider that the losses are only due to the material properties, and not to the fabrication imperfections nor to the tether-induced losses, we can deduce that we can achieve an equivalent Q factor of $Q = (2\pi n)/(\lambda\alpha) = 1900$ with this diamond film, where $n = 2.4$ is the refractive index of diamond, λ is the wavelength, and α is the propagation loss. This estimate is slightly pessimistic since obviously some of the losses come from fabrication imperfections and not from the material. Higher Q factors are thus expected from PhC cavities for which the etching process has been optimized.

We measured PhC cavities with a period $a = 580$ nm. Figure 4 shows the transmission spectrum of two structures exhibiting a 15-nm shift of the central holes for a TE polarization (E field parallel to the plane of the PhC). One cavity (blue curve) has a short barrier of 6 periods while the second has a 10-period long barrier (red curve). For wavelengths below 1575 nm, where the photonic crystal acts as a waveguide, a fiber-to-fiber transmission of -27 dB is observed. The TE photonic band gap in the diamond PhC waveguide is seen for wavelengths above 1588 nm where the transmission remains below -45 dB. When the barrier length of the cavity is varied from 6 to 10 periods, the transmission peak near 1584 nm is reduced from -30 dB to -40 dB while at the same time the full width at half maximum is reduced from 1.7 nm to 0.56 nm. This peak is clearly associated with the cavity mode as confirmed from the observation of the emitted light from the surface here observed using an infrared camera. Moreover, the stability of the resonance frequency from one cavity to the other indicates a good fabrication

reproducibility. The quality factor for the sample with a longer barrier is above 2800. Considering cavities with small mode volume of $\approx 2(\lambda/n)^3$, this value of the Q factor is much higher than all previously reported measured Q factors in polycrystalline²³ or monocrystalline diamond.²⁴ Q factors of similar magnitude have been achieved for other cavities with larger hole shifts. This low sensitivity to the design parameters as well as the fact that the Q factor values for two very different geometries, a photonic crystal and a suspended waveguide, are of the same order seem to indicate that the Q factor is not limited by the geometrical imperfections of the fabricated PhC holes but rather by the material absorption and scattering. This will be confirmed by the use of diamond films with different grain sizes and surfaces treatments since it is difficult to estimate the roughness induced by the etching process on the whole vertical profile from SEM measurements as well as the refractive index change that may be induced by the etching process on the hole surface.²⁹

In conclusion, we have developed a simple technological processing method enabling the fabrication of diamond PhC cavities and waveguides towards planar photonic circuits. We have reached a record Q factor value of 2800 with a small mode volume of $2.1(\lambda/n)^3$ in a cavity obtained from a local width modulation of a PhC waveguide made from nanocrystalline diamond. By improving the polycrystalline diamond quality and grain size, we expect to reach quality factors above 10 000 with larger grains. The reproducible fabrication of hundreds of cavities with quality factors of a few thousands on two-inch wafers opens the route to many applications not requiring extremely high Q factors including biological sensing with photonic crystals structures.³⁰

X.C. gratefully acknowledges CEA for the support provided for his “Chaire CEA/Université Paris Sud.”

- ¹I. Aharonovich, A. D. Greentree, and S. Praver, *Nat. Photonics* **5**, 397 (2011).
- ²I. Aharonovich, S. Castelletto, D. A. Simpson, C. H. Su, A. D. Greentree, and S. Praver, *Rep. Prog. Phys.* **74**, 076501 (2011).
- ³X. Fan, I. M. White, S. I. Shopova, H. Zhu, J. D. Suter, and Y. Sun, *Anal. Chim. Acta* **620**, 8 (2008).
- ⁴F. Trojanek, K. Zidek, B. Dzumak, M. Kozak, and P. Maly, *Opt. Express* **18**, 1349 (2010).
- ⁵D. J. Spence, E. Granados, and R. P. Mildren, *Opt. Lett.* **35**, 556 (2010).

- ⁶P. E. Barclay, K.-M. C. Fu, C. Santori, and R. G. Beausoleil, *Appl. Phys. Lett.* **95**, 191115 (2009).
- ⁷D. Englund, B. Shields, K. Rivoire, F. Hatami, J. Vuckovic, H. Park, and M. D. Lukin, *Nano Lett.* **10**, 3922 (2010).
- ⁸S. Saada, J. C. Arnault, L. Rocha, B. Bazin, and P. Bergonzo, *Phys. Status Solidi A* **205**, 2121 (2008).
- ⁹H. A. Girard, S. Perruchas, C. Gesset, M. Chaigneau, L. Vieille, J.-C. Arnault, P. Bergonzo, J.-P. Boilot, and T. Gacoin, *ACS Appl. Mater.* **1**, 2738 (2009).
- ¹⁰M. Rabarot, J. Widiez, S. Saada, J. P. Mazellier, C. Lecouvey, J. C. Rousin, J. Dechamp, P. Bergonzo, F. Andrieu, O. Faynot, S. Deleonibus, L. Clavelier, and J. P. Roger, *Diamond Relat. Mater.* **19**, 796 (2010).
- ¹¹H. Y. Tsai, C. J. Ting, and C. P. Chou, *Diamond Relat. Mater.* **16**, 253 (2007).
- ¹²V. R. Almeida, R. R. Panepucci, and M. Lipson, *Opt. Lett.* **28**, 1302 (2003).
- ¹³Z. Han, X. Checoury, D. Néel, S. David, M. El Kurdi, and P. Boucaud, *Opt. Commun.* **283**, 4387 (2010).
- ¹⁴X. Checoury, Z. Han, M. El Kurdi, and P. Boucaud, *Phys. Rev. A* **81**, 033832 (2010).
- ¹⁵X. Checoury, Z. Han, and P. Boucaud, *Phys. Rev. B* **82**, 041308(R) (2010).
- ¹⁶M. P. Hiscocks, K. Ganesan, B. C. Gibson, S. T. Huntington, F. Ladouceur, and S. Praver, *Opt. Express* **16**, 19512 (2008).
- ¹⁷B. J. M. Hausmann, B. Shields, Q. Quan, P. Maletinsky, M. McCutcheon, J. T. Choy, T. M. Babinec, A. Kubanek, A. Yacoby, M. D. Lukin, and M. Loncar, *Nano Lett.* **12**, 1578 (2012).
- ¹⁸T. Asano, B. S. Song, and S. Noda, *Opt. Express* **14**, 1996 (2006).
- ¹⁹B. S. Song, S. Noda, T. Asano, and Y. Akahane, *Nat. Mater.* **4**, 207 (2005).
- ²⁰E. Kuramochi, M. Notomi, S. Mitsugi, A. Shinya, T. Tanabe, and T. Watanabe, *Appl. Phys. Lett.* **88**, 041112 (2006).
- ²¹Z. Han, X. Checoury, L.-D. Haret, and P. Boucaud, *Opt. Lett.* **36**, 1749 (2011).
- ²²Y. Taguchi, Y. Takahashi, Y. Sato, T. Asano, and S. Noda, *Opt. Express* **19**, 11916 (2011).
- ²³C. F. Wang, R. Hanson, D. D. Awschalom, E. L. Hu, T. Feygelson, J. Yang, and J. E. Butler, *Appl. Phys. Lett.* **91**, 201112 (2007).
- ²⁴J. Riedrich-Moeller, L. Kipfstuhl, C. Hepp, E. Neu, C. Pauly, F. Muecklich, A. Baur, M. Wandt, S. Wolff, M. Fischer, S. Gsell, M. Schreck, and C. Becher, *Nat. Nanotechnol.* **7**, 69 (2012).
- ²⁵A. Faraon, P. E. Barclay, C. Santori, K.-M. C. Fu, and R. G. Beausoleil, *Nat. Photonics* **5**, 301 (2011).
- ²⁶S. Tomljenovic-Hanic, A. D. Greentree, C. M. de Sterke, and S. Praver, *Opt. Express* **17**, 6465 (2009).
- ²⁷T. M. Babinec, J. T. Choy, K. J. M. Smith, M. Khan, and M. Loncar, *J. Vac. Sci. Technol. B* **29**, 010601 (2011).
- ²⁸M. Fujita, S. Takahashi, Y. Tanaka, T. Asano, and S. Noda, *Science* **308**, 1296 (2005).
- ²⁹A. Battiato, F. Bosia, S. Ferrari, P. Olivero, A. Sytchkova, and E. Vittone, *Opt. Lett.* **37**, 671 (2012).
- ³⁰M. E. Beheiry, V. Liu, S. Fan, and O. Levi, *Opt. Express* **18**, 22702 (2010).